Excited State Dynamics of Isolated 6- and 8-Hydroxyquinoline Molecules

Jean-michel Mestdagh, Lionel Poisson

Excited state dynamics of isolated 6- and 8-hydroxyquinoline molecules

J.-M. Mestdagh [*] L. Poisson [†*]

Abstract

The photoinduced dynamics of isolated n-hydroxyquinoline (nHQ) molecules (n=6,8) was investigated in femtosecond pump-probe experiments. A qualitative difference was found between 8HQ and 6HQ. After an initial rapid decay corresponding to the departure of the initial wavepacket out of the Franck-Condon region of the excitation, the 8HQ probe signal decays to zero in 0.37 ps whereas a much longer time constant of 10.4 ps is observed in 6HQ. This interrogates on the role played by the intramolecular H-bond N$\cdots$HO which is at play the 8HQ molecule. *Ab-initio* were performed at the MCSCF/aug-cc-pVDZ level on the 8HQ molecule to help the discussion. A complex energy landscape was found, which includes a conical intersection.

1 Introduction

Bi-functional molecules which carry both a proton (or H-atom) donor and a proton (or H-atom) acceptor group have attracted attention very early because of their key role in photochemistry and photobiology [1, 2]. The n-hydroxyquinoline molecules belong to this class of molecules. They carry a hydroxyl and an imine group which make them amphoteric, the former group being weakly acidic in the ground electronic state and the second weakly basic. The amphoteric character is enhanced upon electronic excitation and formally the hydroxyl proton (or H atom) can transfer to the imine group. A fundamental aspect is that the H-atom (or proton) is transferred between H-bonded groups [3]. Note that no distinction is made below whether a proton or a H-atom is transferred. We simply indicate that a H-atom transfer is at play. This is justified by the fact that this distinction is not as pregnant in the gas phase (see below) as in solvents.

The photoinduced tautomerization of n-hydroxyquinoline molecules has motivated a series of studies in many laboratories. For instance, Olivier Poizat and coworkers have performed picosecond transient absorption spectroscopy experiment on 6-hydroxyquinoline in organic solvents and various aqueous solutions [4]. Too many works have appeared on this question to quote them thoroughly. In all of them, as in the work by Poizat and coworkers, the n-hydroxyquinoline molecules are coupled to an environment: solvents or solutions [5, 6, 7, 8, 9, 10], polymer films [11], cyclodextrin [12] or reverse micelles [13].

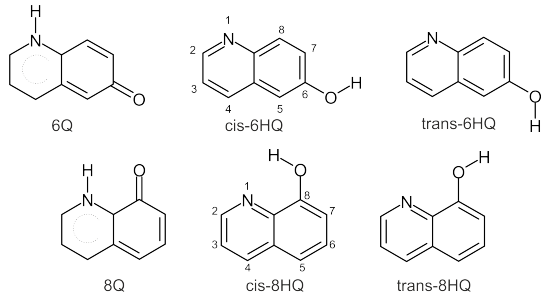

Figure 1: Scheme of the 6-quinolone/cis-6-hydroxyquinoline/trans-6-hydroxyquinoline (top line) and 8-quinolone/cis-8-hydroxyquinoline/trans-8-hydroxyquinoline tautomers (bottom line).

The present work aimed at investigating the in-

[*]LIDYL, CEA, CNRS, Université Paris-Saclay, CEA Saclay 91191 Gif-sur-Yvette France.

[†]corresponding author - lionel.poisson@cea.fr

trinsic photoinduced dynamics of n-hydroxyquinoline molecules, *i.e.* the dynamics of these molecules when free of any environment. The main point was to examine whether electronic excitation can stimulate the exchange of a H atom between the hydroxyl and the imine groups without the participation of an environment which may lower an energy barrier, or offer alternative reaction paths to the direct path.

The comparison between the 6-hydroxyquinoline and the 8-hydroxyquinoline molecules appeared especially relevant for this purpose since an intramolecular H-bond is present between the hydroxyl and imine groups in the latter molecule and not in the former. Two possible geometries of these molecules, that we call *cis*- and *trans*- by convenience and the relevant tautomers, 6-quinolone and 8-quinolone, where the H-atom transfer is achieved are drawn in Fig. 1. Hereafter, n-hydroxyquinoline/n-quinolone tautomers are labeled nHQ/nQ, where n labels the C atom which caries the O atom. The atom numbering is given in Fig. 1.

Gas phase isolation of the nHQ molecules in a setup which associates a molecular beam, femtosecond lasers and a velocity-map imaging (VMI) detection is the dedicated technique to observe the early instants of the photoinduced dynamics of these molecules in the absence of coupling with an environment. Accordingly, the specie under study is isolated in the vacuum. At time zero, it is electronically excited to the desired state by absorption of a photon from an ultrashort (femtosecond) laser pulse (the pump laser). After a certain time delay τ, the specie of interest is interrogated to get as much information as possible on its chemical nature and quantum state. This is achieved by adapting mass spectrometry and photoelectron spectroscopy to real-time measurements. An ultrashort laser pulse (probe laser), generally of a different wavelength than that of the pump laser, is used to ionize the specie under study at time τ. When the extracting plates are tuned to detect photoelectrons (resp. photoions) and the appropriate data treatment is performed, photoelectron energy spectra (resp. a mass spectrum) are recorded as a function of τ. This documents both the chemical nature of the specie that is ionized by the probe laser and its electronic state (or superposition of electronic states) as a function of τ. This kind of setup is routinely used in the domain of gas-phase femtochemistry. In the present work, it was operated with pump pulses at 266 nm and probe pulses at 800 nm. Also, the VMI was tuned to detect photoelectron only and a standard time-of-flight spectrometer was added to mass analyse the photoions. The pump pulses acted through single photon excitation and formed a vibrational wavepacket in the S_1 state of the nHQ molecules under study. The subsequent wavepacket evolution was followed as a function of τ by multiphoton ionization with the time delayed probe pulses.

The experimental information was complemented by *ab-initio* calculations to map semiquantitatively the energy landscape of 8HQ/8Q which is involved in the pump-probe process. Accordingly, electronic excitation and ionization energies were computed along a reaction path where the hydroxyl H-atom of 8HQ is transferred to the imine group, hence forming 8Q. Three calculations were performed according to whether the geometry optimization along the reaction path minimizes the ground electronic state S_0, the first electronically excited state S_1 or the ground ionic state D_0. These calculations were performed at a semiquantitative level of theory. The vertical excitation and ionization energy of 6HQ/6Q and 8HQ/8Q were examined in a separate calculation at a higher level of theory.

2 Results

2.1 Photoelectrons

The experimental work has started with the femtosecond Time Resolved PhotoElectron Spectroscopy(fs-TRPES) investigation of the 6HQ and 8HQ molecule as explained in the Technical Section (Sec. 5). A series of photoelectron images (raw-VMI-images) were recorded at various pump-probe time delays ranging from -500 fs to +470 ps. As explained in Sec. 5, each raw-VMI-image was reconstructed using the pBasex algorithm to get the corresponding VMI-distribution. This provided us with the three quantities $I_0(E,\tau)$, $I_2(E,\tau)$ and $I_4(E,\tau)$ where E is the kinetic energy of the photoelectrons and τ the pump-probe time delay.

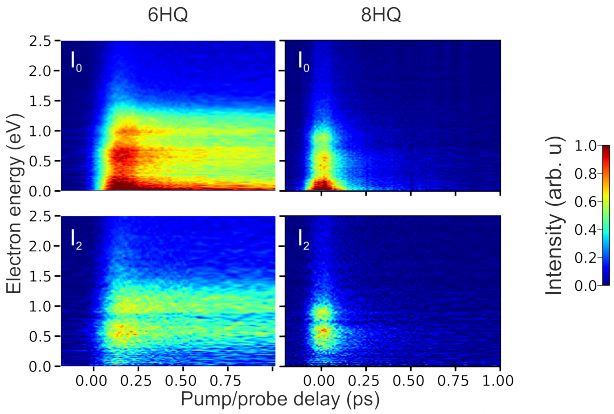

Figure 2: 6HQ (left) 8HQ (right) : 3D-plot of the $I_0(E,\tau)$ and $I_2(E,\tau)$ quantities extracted by the p-Basex algorithm from raw-VMI-images recorded in a 266/800 nm pump/probe experiment. The horizontal scale in each panel is the pump-probe time delay (in ps), the vertical scale, the photoelectron energy E (in eV) and the color scale, the photoelectron intensity (in arbitrary units). The color code for intensities is given on the right of the figure.

The $I_4(E,\tau)$ signal was always very weak and is not reported here. The other two quantities are shown as 3D-plots (τ, E, Intensity) in the left (resp. right) column of Fig. 2 for 6HQ (resp. 8HQ). Note that the three scales (energy, time delay and signal intensity) is the same in the four panels of the figure.

Each panel of the figure shows the relevant photoelectron spectrum (vertical scale, intensity) as a function of the time delay τ (horizontal scale). Only the first 1 ps appears in the figure. A qualitative difference is immediately apparent when comparing the 8HQ and 6HQ molecules. With 8HQ, the $I_0(E,\tau)$ and $I_2(E,\tau)$ quantities decay rapidly within the 1 ps time window of the figure, whereas with 6HQ, these quantities are extending beyond 1 ps. They were still significant up to 470 ps.

The 3D-plots reported in Fig. 2 contain the essential information regarding the photoinduced dynamics of the 6HQ and 8HQ molecules, *i.e.* the time evolution of the photoelectron spectra. The latter reflect the time evolution of the excited wavepacket that is probed. A common assumption is to describe such an evolution as a sequential population transfer from one transient to the other. Here, we found enough to consider three transients:

$$\mathrm{A} \xrightarrow{\tau_1} \mathrm{B} \xrightarrow{\tau_2} \mathrm{C} \qquad (1)$$

where τ_1 and τ_2 are the corresponding decay time constants. Transient A stands for the initial wave packet generated by the pump laser pulse, whereas transient C is the final step of the wavepacket evolution, when the available electronic energy is too small to allow for a measurable photoionization signal by the probe laser. Transient B is a landmark along the wavepacket evolution. Unraveling its nature is discussed below.

A way to extract the desired information from Fig. 2 is to reconstruct each 3D-plot, *i.e.* to fit the $I_p(E,\tau)$ quantities by a linear combination of the type

$$I_p(E,\tau) = \sum_{i=A,B} f_p^i(E) \times n_i(\tau), \qquad (2)$$

where $n_i(\tau)$ is the population of the transient A or B at delay time τ, and $f_p^i(E)$ the photoelectron spectrum of each transient i=A or i=B for photoelectrons distributed as the Legendre polynomial of order p. Transient C does not appear in Eq. 2 since has a too small electronic energy to be detected by photoionization (see its definition in Eq. 1). In short, Eq. 2 assumes that at each delay time, the observed photoelectron spectrum is the superposition of two spectra, that of A and that of B in a ratio that depends on the delay time through the populations $n_{A,B}(\tau)$. The latter are are provided by algebraic integration of the differential equations describing the kinetic model (see Eq. 1). The decay times τ_1 and τ_2 that appear in the $n_{A,B}(\tau)$ expressions are considered as fit parameters. A time convolution is included into the integration to account for the cross correlation function between the pump and probe pulses (about 80 fs). We found convenient to include the time origin t_0 (zero delay time between the pump and the probe) as further parameter in the fit procedure which reconstructs the 3D-plots of Fig. 2.

Reconstruction of the 3D-plots based on an optimization of the $n_i(\tau)$ functions through the three pa-

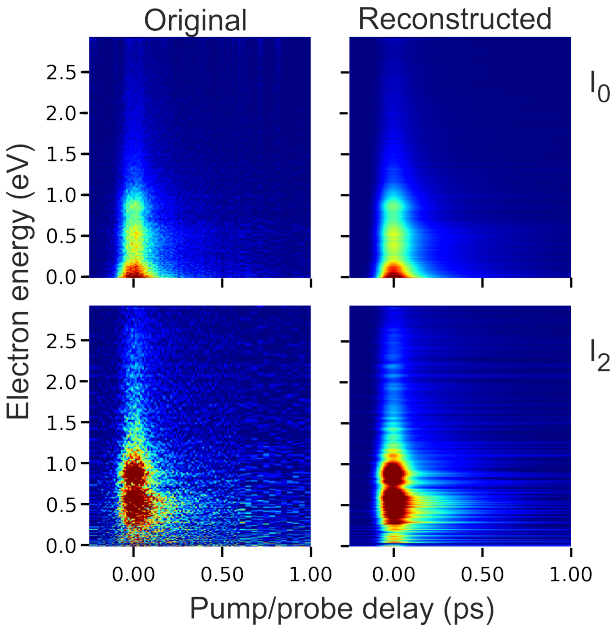

Figure 3: Comparison between reconstructed (right panels) and original 3D-plots taken from Fig. 2 for the 8HQ molecules (left panels). The top panels (resp. bottom) shows I_0 (resp. I_2) plots.

rameters τ_1, τ_2 and t_0. In practice, given a set of these parameters, an algebraic parsimonious adjustment of the $f_p^i(E)$ spectra is performed on the whole 3D-plot as described by Mortada *et al.* [14]. This provides a first guess of the reconstructed plot. Then, a least square procedure minimizes the residue between the reconstructed and the original 3D-plot. The basis set used for the parsimonious adjustment includes the time evolution of the populations of transients A and B ($n_{A,B}(\tau)$) and a constant for adjusting the background. A Singular Value Decomposition (SVD) analysis was used to get the weight of each $n_{A,B}(\tau)$ curve as a function of the photoelectron energy E. The latter quantity represents the desired photoelectron spectrum $f_p^{A,B}(E)$.

In brief, the present parsimonious adjustment/SVD procedure provides all the information on the dynamics, *i.e.* both the $f_p^{A,B}(E)$ spectra (i=A and B) and the time constants τ_1, τ_2. It is actually

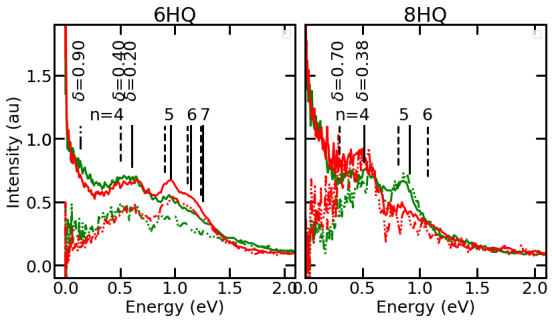

Figure 4: Photoelectron spectra $f_p^A(E)$ of transient A in green (resp. $f_p^B(E)$ in red) for those electrons distributed as Legendre polynomial P_0 (p=0, full curves) and P_2 (p=2, dashed curves). They are provided by the parsimonious adjustment/SVD procedure as described in the text. The vertical lines show the expected resonances of the probe laser with Rydberg states of principal quantum number n and quantum defect δ as labeled in the figure.

fairly similar to the data analysis described by Ruckebusch *et al.*[15] or by Panman *et al.*[16] in the context of Time-resolved vibrational spectroscopy. Its reliability for reconstructing the 8HQ 3D-plots can be appreciated in Fig. 3. A reconstruction of similar quality was achieved for the 6HQ 3D-plots. The corresponding photoelectron spectra $f_p^{A,B}(E)$ are shown in Fig. 4 and the time constants τ_1 and τ_2 in Tab. 1.

Molecule	τ_1 (ps)	τ_2 (ps)
6HQ	0.16	10.4
8HQ	0.053	0.37

Table 1: Time constants τ_1, τ_2 provided by the parsimonious adjustment/SVD procedure.

2.2 Photoions

Time-of-Flight (TOF) mass spectra were recorded in both the 6HQ and 8HQ experiments as a function of the pump–probe time delay τ. Their sum over τ is

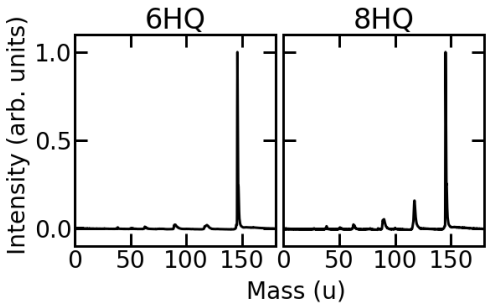

Figure 5: Mass spectra of the 6HQ (left panel) and 8HQ (right) molecules.

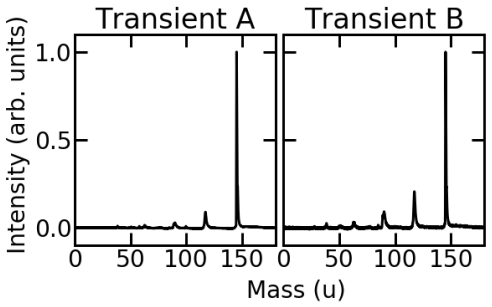

Figure 6: Mass spectra of the A (left panel) and B (right) transients in the 8HQ experiment. The spectra were provided by the parsimonious adjustment/SVD procedure applied to photoion 3D-plots that are not shown here.

shown in Fig. 5. The main peak at mass 145 u in each spectrum corresponds to the parent ion. The fragment masses are the same in both experiments but the fragmentation is significantly more efficient with 8HQ. The main fragment at 115±2 u is significantly broader than the parent peak. This is barely visible with the scale of the figure. This peak is likely associated with the loss of CO. Peaks of smaller masses are observed at 90 u, ∼63 u,...

Given the larger fragmentation in the 8HQ experiment, a more elaborated data treatment was performed. Plotting the mass spectra as a fonction of the pump-probe time delay provided 3D-plots similar as those of Fig. 2, except the vertical scale is a photoion mass spectrum instead of a photoelectron energy spectrum. A similar parsimonious adjustment/SVD procedure as above was used to reconstruct the photoion 3D-plots. However, less parameters are included in the adjustment since the time constants listed in Tab. 1 does not need to be adjusted again. The output of this data analysis is the mass spectrum of the transients A and B shown in Fig. 6. The two mass spectra look the same but the fragment peaks are more intense with transient B than with transient A. When bringing this figure (mass spectra) together with Fig. 4 (photoelectron spectra), a full experimental characterization of transients A and B is obtained.

	S_0	$S_0 \rightarrow S_1$	$S_0 \rightarrow S_2$	$S_0 \rightarrow D_0$
6Q	0.97	2.155	2.901	5.369
cis-6HQ	0	4.356	5.513	7.010
trans-6HQ	-0.02	4.418	5.061	7.036
8Q	0.73	1.764	3.258	5.357
cis-8HQ	0	4.016	5.102	7.576
trans-8HQ	0.34	4.073	5.417	7.638

Table 2: Relative energies (in eV) of the *cis*-nHQ, nQ and *trans*-nHQ (n=6 and 8) molecules, their geometries being optimized at the MP2/aug-cc-pVDZ level of theory (second column). The *cis*-nHQ energy is taken as reference. The other columns report CAS(12,12)/aug-cc-pVDZ vertical excitation (column 3 and 4) and ionization (last column) energies from the optimized S_0 state of each molecule.

2.3 Calculation

The calculation methodology described in the Technical Section (Sec. 5) was used to predict the relative energetics of the of *cis*-nHQ, *trans*-nHQ and nQ (n=6 and 8) molecules at the MP2 and CAS(12,12)/aug-cc-pVDZ level of theory. The results are shown in Tab. 2.

Fig. 7 reports the relative energy of the S_0, S_1, S_2, D_0 and D_1 levels of the 8HQ/8Q molecules along a reaction path that connects *cis*-8HQ to 8Q. This path is defined in the Technical Section (Sec. 5). The calculation were performed at the CAS(2,2)/cc-pVDZ

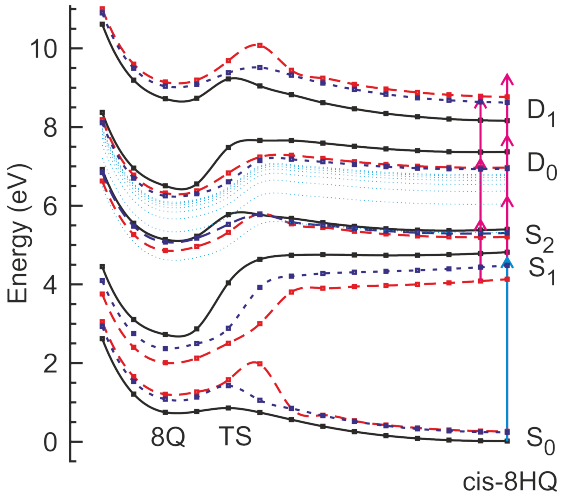

Figure 7: Energy of the S_0, S_1, S_2, D_0 and D_1 levels along a tentative reaction path connecting cis-8HQ (right hand side of the plots) to 8Q through a transition state TS. The black/solid (resp. red/long dashed and blue/short dashed) curves show the energy profiles when the molecular geometries are optimized for the S_0 (resp. S_1 and D_0) state. See the technical section for details.The thin cyan dotted curves show Rydberg states (n=3-10) converging to the optimized D_0 state, assuming a δ=0.1 quantum defect. The blue vertical arrow show the energy of the pump photon and the pink arrows that of the probe photons.

level of theory. Three curves are shown for each level whether the molecular optimization was performed for the S_0, S_1 or D_0 state. These calculations must be considered as semiquantitative and meant as guidelines for the discussion.

3 Discussion

A preliminary remark must be done from the calculations reported in Tab. 2. Strikingly, the $S_0 \rightarrow S_1$ excitation energy of the 6Q and 8Q molecules is much lower than that of the corresponding *cis*-nHQ and *trans*-nHQ molecules. The H-atom transfer from the hydroxyl to the imine group is therefore exothermic along the S_1 potential energy surface: ΔE=-1.53 eV for *cis*-6HQ→6Q and -1.52 eV for cis-8HQ→8Q. The reverse is predicted along the ground electronic state surface (respectively 0.97 and 0.73 eV). This illustrates the statement made at the beginning of the introduction that electronic excitation enhances the amphoteric character of the nHQ molecules. In that sense, the H-atom transfer from the hydroxyl to the imine group is stimulated by the electronic excitation.

The calculations reported in Tab. 2 show that *cis*-8HQ is significantly stabilized with respect to both *trans*-8HQ and 8Q. This makes that the 8HQ experiment necessarily proceeds from *cis*-8HQ. In contrast, *cis*-6HQ and *trans*-6HQ have about the same energy, suggesting that the 6HQ experiment proceeds from both geometrical isomers.

An important observation in Fig 4 concerns the shape of the $f_0^{A,B}$ photoelectron spectra in Fig 4. They are broadly structured. This can be understood as revealing a series of broad peaks superimposed on a featureless decay starting at a zero energy and extending up to 1.5 eV or more. Such a shape is common in the present kind of experiments where the probe laser acts through multiphoton ionization. For instance, this was observed in our work on the 2-hydroxypyridine dynamics [17] and in that of Bohl *et al.* on the coronene photionization.[18] Its interpretation is given in the latter works: *i)* The featureless decay appears because part of the ionization proceeds by evaporation of thermal electron upon autoionization of the superexcited molecule which has absorbed three (or more) non resonant probe photons; essentially isotropically distributed photoelectrons are expected for this process, in agreement with the fact that the featureless decay is almost not existing in the $f_2^{A,B}$ spectra (see Fig 4). *ii)* The structure of peaks appear upon the resonant absorption of two probe photons by a Rydberg state followed by a direct single photon ionization. This phenomenon is know as "*Rydberg Fingerprint Spectrocopy*" [19]. Possible resonances which match the observed peaks are indicated by vertical line in Fig 4. They are located using the simple Rydberg formula $IE - \frac{R}{(n-\delta)^2}$ where IE is the ionization energy of the species of interest, n the principal quantum number and δ the quantum defect of the Rydberg series under consideration. Strongly

overlapping resonances between ns (δ=0.7-0.9), np (δ=0.4) and nd (δ=0.2) Rydberg states with n=4-7 are suggested by the figure. Note that such an overlap precludes a detailed analysis based on "*Rydberg Fingerprint Spectrocopy*" as done in our work on the 2-hydroxypyridine dynamics.[17] To a large extent, this difficulty was bypassed here by the parsimonious adjustment/SVD procedure which allowed us documenting the photoelectron spectrum of transients A and B.

The dominant effect of autoionization/evaportaion (featureless decay) and Rydberg fingerprint (broad peaks) processes on $f_{0,2}^{A,B}$ spectra significantly complicates the interpretation of their shape in terms of dynamics of the neutral electronically excited nHQ molecule that is the subject of the present investigation. These shapes are affected indeed by the dynamics mediates ionization by the probe laser: evaporation dynamics of the superexcited state for the featureless decay; dynamics within the intermediate Rydberg state for the broad peaks. These dynamics are initiated during the ionization step and are therefore not expected to be affected dramatically by varying the pump-probe delay time τ. Hence, although the exact shape of the $f_{0,2}^{A}$ or $f_{0,2}^{B}$ spectra is not relevant for discussing the dynamics of the neutral electronically excited nHQ molecule, the shape differences between the $f_{0,2}^{A}$ and $f_{0,2}^{B}$, *i.e.* the deformation of the overall photoelectron spectrum as a function of τ, likely reflects the desired information. Our work on the 2-hydroxypyridine dynamics exemplifies this possibility in a context where only the overall photoelectron spectrum is documented.[17] The situation is richer here since the $f_{0,2}^{A}$ and $f_{0,2}^{B}$ spectra were extracted explicitly from the overall photoelectron spectrum. The discussion below takes advantage of this opportunity.

We come now to the centre of the discussion. It concerns the qualitative difference observed between the 6HQ and 8HQ dynamics: both the photoion and the photoelectron probe signals decay to zero in less than 1 ps with 8HQ, whereas a much slower decay is observed with 6HQ. This appears quantitatively in Tab 1, the time constant of the the slow decay being 10.4 ps for 6HQ and 0.37 ps for 8HQ.

A direction for rationalizing this observation is to note the proximity between the imine and hydroxy groups in *cis*-8HQ which does not exist in either *cis*-6HQ or *trans*-6HQ. In *cis*-8HQ, a five member ring NCCOH closed by an intramolecular H-bond N$\cdots$HO (for *cis*-8HQ) or NH$\cdots$O (for 8Q) stabilizes the structure. This appears clearly in Tab. 2. In 6HQ, where no intramolecular H-bond is anticipated, the computed energy difference between *cis*-6HQ and *trans*-6HQ is essentially zero (more precisely, within the expected calculation uncertainties). In contrast, *cis*-8HQ, where such a bond is present, is stabilized by 0.34 eV with respect to *trans*-8HQ where no such bond exists. Importantly, Tab. 2 suggests that the intramolecular H-bond in *cis*-8HQ also stimulates the ground state H-atom transfer reaction which transforms *cis*-8HQ into 8Q. The latter reaction is indeed less endoenergetic (0.73 eV) than the corresponding one for the *cis,trans*-6HQ to 6Q transfer (0.97 eV).

It is very tempting at this point to associate the rapid decay of the photoelectron and photoion signals observed in the photoinduced dynamics of 8HQ (compared to that of 6HQ) to the mediating effect of intramolecular the H-bond. Let-us examine this in more details by first discussing the predictions of the computational data in Tab. 2 and Fig. 7.

The vertical excitation energies listed in Tab. 2 suggest that the pump photons at 266 nm (4.66 eV) excite the 6HQ and *cis*-8HQ in the S_1 state with a significant internal energy (0.3 eV for 6HQ; 0.6 eV for *cis*-8HQ). Energetically, the S_2 state cannot be accessed initially. Also, it is seen from Fig. 7 that the probe photons at 800 nm (1.55 eV) likely operate through 2- or 3-photon processes to ionize the nHQ/nQ system in its way from nHQ to nQ as it is still in the S_1 state.

From Tab. 2, photoelectron energies up to 2.0 eV are expected for the 3-probe photon ionization of *cis*-6HQ (resp. 1.10 eV for *cis*-8HQ). Smaller energies are expected for detection of 6Q and 8Q: up to 1.44 eV and 1.06 eV, respectively. These numbers should be considered as lower bounds of the expected energies since the calculated energies of the D_0 states correspond to the optimized geometry of S_0 states. Nevertheless, we do not think that this modifies the ordering between the expected photoelectron ener-

gies and the following qualitative analysis applies. When the H-atom transfer is achieved, the expected energy of the photoelectrons is reduced, especially for the 6HQ/6Q system. This tendency can be followed along the reaction path for 8HQ/8Q in Fig. 7. Whatever the optimization that is chosen, the energy of the S_1 state decays steadily from *cis*-8HQ to 8Q whereas a transition state is observed along the D_0 curve. This predicts that the photoelectron energy decreases as the wavepacket that is probed proceed along the H-atom transfer coordinate.

A very unexpected observation is made when turning to the photoelectron spectra of transient A (green curves) and B (red curves) in Fig. 4. The A spectra of 8HQ (top right panel) have a bump centred at 0.85 eV which is essentially absent in the B spectra. The reverse is observed in 6HQ. It is also interesting to observe that the peak near 0.5 eV in the 8HQ spectra is enhanced from A to B whereas the opposite behavior is observed in 6HQ. The different behaviour of the average photoelectron energy suggests that the electronic configurations involved in the transient B detection are not the same whether 6HQ or 8HQ is considered.

Let us first bring together the computational energetics discussed above for 6HQ/6Q and the experimental observation. The computation indicates a reduction of the photoelectron energy when 6Q is probed instead of 6HQ, whereas the experiment suggests the opposite behavior: features of large energy are favored over those of small energy when switching from A to B in the spectra shown in Fig. 4. Transient B which is populated by the decay of A is thus unlikely associated with the formation of 6Q.

The following picture emerges for the 6HQ dynamics. Transient A represents the initial wavepacket when the pump laser excites *cis*-6HQ in the S_1 state. Transient B then likely represents the wavepacket as it has moved out of the Franck-Condon region and has spread over the S_1 potential energy surface. Along this picture, the time constant of 0.16 ps given in Tab. 1 for transient A would be the timescale for the wavepacket to move out of the Franck-Condon region. The longer time constant of 10.4 ps given to transient B would then be the time needed for the wavepacket to explore the S_1 potential energy surface and find its way to the ground electronic energy surface (the undetected transient C) where the H-atom transfer may occur. When the wavepacket crosses the latter location, it evolves certainly very rapidly. Because this rapid evolution follows a slow dynamics, it cannot be probed efficiently and does not lead to the apparition of an observable feature in the photoelectron spectrum. No transient C can be detected, even for a very small duration. This question is examined again at the end of the discussion.

An apparently similar roaming behavior has been reported in our work on the excited state dynamics of 2-Hydroxypyridine. [17] Nevertheless, the time scale of the roaming behavior is much longer here: 10.4 ps *versus* 1.3 ps.

We turn now to the 8HQ/8Q dynamics. It was discussed above that the maximum photoelectron energy that is expected from Tab. 2 for photoionizing 8HQ and 8Q is 1.10 and 1.06 eV, respectively. This difference is far too small, within calculation errors, to help deciding whether transient B is associated with 8HQ or 8Q. Importantly, the difference between the green (transient A) and red (transient B) spectra which favors low energy features in the transient B spectra is consistent with the reduction discuss above of the photoelectron energy when the wavepacket proceeds towards 8Q along the 8HQ-8Q reaction path.

A simple assumption at this point is to imagine a similar situation for 8HQ/8Q as that above for 6HQ/6Q where Transient A represents the initial wavepacket in the Franck-Condon region and Transient B the wavepacket as it spreads on the S_1 potential energy surface. The question is why the lifetimes of Transients A and B are so short with 8HQ/8Q.

Fig. 7 reveals two interesting features on the 8HQ/8Q surface: *i)* no barrier is present, *i.e.* the potential energy decreases steadily between 8HQ and 8Q along S_1; *ii)* a bump is present along S_0 and make S_0 close to S_1 when the reaction path is optimized to minimize S_1 (red curves). We interpret the latter feature as the vicinity of a conical intersection between the S_0 and S_1 potential energy surfaces. No attempt was made to scrutinize the exact location of the conical intersection. Nevertheless, these two features help us refining the picture of the 8HQ

dynamics and putting it in perspective with that of 6HQ. The steady slope that is predicted by the calculation along the reaction path of the 8HQ/8Q system is likely due to the presence of the intramolecular H-bond and may not exist in 6HQ/6Q where no such bond exists. The latter expectation is consistent with the three time shorter lifetime of A in 8HQ than in 6HQ (0.053 ps *versus* 0.16 ps, see Tab. 1). Along this picture, the slope along the S_1 surface in 8HQ/8Q drives the wavepacket near the conical intersection where it is rapidly transferred to the ground state surface and potentially to the transfer reaction of the H-atom. From the assumption done for building the reaction-path in Fig. 7 this movement of the wavepacket involves essentially the displacement of the H-atom. The more efficient fragmentation observed in Fig. 6 for transient B is an indication that upon ionization by the probe laser, the ions that are formed when the H-atom is on his way between the O- and the N-atom (transient B) contain more internal energy than ions formed when the H-atom is still in the Franck-Condon region of excitation by the pump laser (transient A). Because the H-atom is very light, the displacement along the reaction path may be very rapid and account for the 0.37 ps lifetime of transient B.

Actually, a conical intersection may exist in 6HQ also and its access involves also the displacement of the H-atom. The much slower dynamics that is observed indicates that if existing, such a conical intersection cannot be accessed directly, essentially because no intermolecular H-bond is present to configure adequate slopes in the S_1 surface. Hence, the electronically excited 6HQ/6Q system experiences a roaming dynamics where the conical intersection is found after a long time.

4 Summary and conclusion

The photoinduced dynamics of isolated 6-hydroxyquinoline (6HQ) and 8-hydroxyquinoline (8HQ) molecules was investigated in a molecular beam setup coupled to a pulsed femtosecond pump-probe laser facility. The pump pulses (266 nm) excited these molecules to the S_1 state, whereas time delayed probe pulses (800 nm) interrogated the subsequent dynamics in a 2- or 3-photon ionization process. The resulting photoelectrons and photoions were detected separately. Accordingly, the energy and angular distributions of the photoelectrons and the mass spectrum of the photoions were recorded as a function of the pump/probe time delay.

A specific treatment was applied to these data. It couples Singular Value Decomposition (SVD) and Parsimonious Adjustment (PA) and allowed us extracting all the information pertaining to the kinetic model used to describe the dynamics that is probed. The model assumes that three transients A, B and C are at play sequentially: "A" is the initial wavepacket as it is launched by the pump laser in the Franck-Condon region of the S_1 potential energy surface; "C" is the final step of the wavepacket evolution when the electronic energy is too small to allow photoionization by the probe laser; "B" is an intermediate step where the wavepacket has spread over the S_1 potential energy surface before it decays to "C".

The beauty of this data treatment was to provide us with the photoelectron and mass spectra of transients A and B as a function of the pump-probe delay between the pump and probe pulses. This information can be considered as an almost full experimental characterization of the photoinduced dynamics of the 6HQ and 8HQ molecules under investigation. A step further would be a correlated information between the photoelectron and photoions generated by the probe laser. This was precluded with the present laser system, whose recurrence is 20 Hz only.

Ab-initio calculations were performed at various level of theory (CAS(2,2)/cc-pVDZ, MP2/aug-cc-pVDZ and CAS(12,12)/aug-cc-pVDZ) to help the discussion. Beyond energy considerations regarding the nature of the excited energy level that is probed (S_1), the number of probe photon needed for the detection (2 or 3) and the possibility of probing through Rydberg resonances, an important information concerns the H-atom transfer reaction where the H-atom of the hydroxyl group in 8HQ switches to the imine group and forms 8-quinolone (8Q). A complex energy landscape was found where slopes created by the intramolecular H-bond drive the electronically excited wavepacket to the vicinity of a conical intersection

where it switches to the ground electronic surface.

Importantly, a reliable picture of the 6HQ and 8HQ dynamics cannot be drawn from either the sole experimental or the sole computational information mentioned above. Such a situation is common in gas phase reaction dynamics studies when sub-picosecond wavepacket evolutions are followed in middle size molecules (10-30 atoms). The complementarity between both approaches is necessary.

In both the 6HQ and 8HQ molecules, transient A decays into B with a much smaller time constant τ_1 than B into C (time constant τ_2). In spite of this similarity, the dynamics of 6HQ and 8HQ are qualitatively different, τ_1 and τ_2 being much larger in 6HQ than in 8HQ (0.16 and 10.4 ps *versus* 0.053 and 0.370 ps, respectively). This interrogates on the role played by the intramolecular H-bond N$\cdots$HO, which is present between the hydroxyl and imine groups of 8HQ. A clue is provided by the calculations performed on the 8HQ/8Q system. Slopes, whose existence is likely related the H-bond, exist in the S_1 potential energy surface of this molecules and offer a direct path to the excited wavepacket formed by the pump laser to a conical intersection where it can switch to the ground state energy surface, possibly forming the H-atom transfer product 8Q. A similar situation is unlikely in the 6HQ/6Q system where no such intramolecular H-bond is present. Then, a roaming dynamics associated with much larger time constants would be a play.

5 Technical section

5.1 Chemicals

The present work was initiated in collaboration with Olivier Poizat, who provided us with the nHQ molecules. As described in Ref. [4], they were commercial products (Kodak, Sigma) either recrystallized from ethyl ethanoate or purified by vacuum distillation.

5.2 Experimental setup

A detailed description of the experimental setup appears in former publications of our group [20, 21, 22]. The setup was installed on the femtosecond SLIC/LUCA laser facility at CEA Saclay[1].

Briefly, the desired nQ/nHQ molecules were seeded into a pulsed molecular beam operating with helium at a repetition rate of 20 Hz. The molecular beam crossed pulsed femtosecond pump and probe laser beams at right angles. The co-propagating laser beams were overlapped spatially.

The pump pulses (266 nm wavelength) excited the nQ/nHQ molecules electronically whereas the probe pulses (800 nm wavelength) allowed us monitoring the resulting nQ/nHQ dynamics through ionization. The time delay between the pump and probe laser pulses could be varied over a 1 ns range using a delay line. The cross-correlation between the laser pulses was 80 fs. This fixed the time resolution of the experiment. Finally, both lasers were linearly polarized and importantly, the polarization of the probe laser was within the plane defined by the molecular and laser beams.

5.3 Probing photoelectrons

A Velocity Map Imaging (VMI) detector, designed as described by Eppink and Parker, [23] was used to detect the photoelectrons. The latter were extracted perpendicularly to both the molecular and the laser beams and fs-TRPES experiments could be performed as described by Stolow *et al.* [24].

Raw 2-dimensional photoelectrons images were collected by the VMI as a function of the time delay τ between the pump and probe laser pulses. We call them raw-VMI-images. This provided us with the 2D-projection of the 3D energy and angular distributions of the photoelectrons, which represents the full information on the photochemical process that was probed. The scrambled information on these distributions that was present in the raw-VMI-images must therefore be disentangled. The pBasex algorithm was used for this purpose. [25] It reconstructs

[1] http://iramis.cea.fr/slic/

the VMI-distribution from the measured raw-VMI-images.

The pBasex algorithm is based on the inverse Abel transform and takes advantage that the angular distribution of the photoelectrons has a cylindrical symmetry about the polarization of the probe laser, the latter being perpendicular to the extraction axis of the VMI. As a result of the cylindrical symmetry, the 3D angular distribution of the photoelectrons can be described by a single polar angle: the angle θ between the scattering direction of the photoelectrons and the laser polarization. Within the pBasex algorithm, this distribution was expended on a basis of Legendre polynomials P_p. Since the probe laser was linearly polarized, only even orders appear: p=0,2,4,... A raw-VMI-image, which was recorded at time delay τ was therefore reconstructed as a VMI-distribution given by $I(R,\theta,\tau) = I_0(R,\tau)\big[1+\beta_2(R,\tau)\,P_2(\cos\,\theta)+ \beta_4(R,\tau)\,P_4(\cos\,\theta) + ...\big]$ where R and θ are the polar coordinates of the photoelectrons in the VMI-distribution and τ the pump-probe delay. The polar radius R is a function of the kinetic energy of the detected photoelectron. A separate experiment was performed where the nHQ molecules are replaced by O_2 molecules, which are ionized by multiphoton absorption of the probe laser. The well-known ionization energetics of O_2 was used to relate the R scale to a scale of kinetic energy E [26].

In the present work the Legendre expansion was limited to p=4. Hence, the pBasex treatment of the raw-VMI-images provided us with three sets of quantities $I_0(E,\tau)$, $I_2(E,\tau)=I_0(E,\tau)\times\beta_2(\tau)$ and $I_4(E,\tau)=I_0(E,\tau)\times\beta_4(\tau)$. $I_0(E,\tau)$ refers to photoelectrons isotropically distributed and documents the energy spectrum of these photoelectrons as a function of the time delay τ. $I_2(E,\tau)$ (resp. $I_4(E,\tau)$) provides the same kind of information for the photoelectrons distributed as the Legendre angular distribution of second (resp. fourth) order.

5.4 Probing photoions

A linear Time-Of-Flight (TOF) mass spectrometer was used to collect the mass spectra. The corresponding measurements document the signal intensity of mass selected ions as a function of the pump-probe time delay τ.

5.5 Computation technique

The MOLPRO quantum chemistry package [27] was used for conducting *ab initio* calculations on the S_0, S_1, S_2, states of 8Q/*cis*-8HQ/*trans*-8HQ. The D_0 and D_1 states of the corresponding ions were documented also.

A first series of geometry optimizations were performed without geometry constraint at the MP2 (Second order closed shell Møller-Plesset perturbation theory [28]) level of theory using the augmented correlation-consistent double-zeta (aug-cc-pVDZ) basis set [29]. This provided us with a first guess of the structure of the 8Q, *cis*-8HQ and *trans*-8HQ tautomers. As expected from the chemical intuition, planar geometries were found. With difficulty, the transition state between 8Q and *cis*-8HQ was searched. Again, in consistency with the chemical intuition, a planar geometry was found.

Given this information, a reaction path was built to follow the H-atom transfer from 8HQ to 8Q. Within a Z-matrix representation of the molecular system, this was achieved by varying the N-H distance between 2.08 and 0.9Å, assuming that the molecule stays planar. All other coordinates but the C-H distances were optimized along this path. The optimization was performed by using energies provided by state-averaged MCSCF/MULTI calculations [30, 31] as input into OPTG program. The MULTI program was operated as a 2-state (S_0, S_1) averaged CAS(2,2) (two electron in two orbitals), using the cc-pVDZ basis set. Three optimizations were conducted. In the first two, the ground electronic energy S_0 and the first excited electronic state S_1 were used as input by the OPTG program. For the third one, a separate CAS(1,2) calculation was performed using the ground state ionic energy D_0 as input of the OPTG program. Fourteen points were sampled along the H-atom transfer coordinate.

For each point along the H-atom transfer path a more accurate state-averaged CAS(6,6) was performed using the aug-cc-pVDZ basis. This provided us with three series of potential energy curves (S_0, S_1, S_2, D_0, D_1) which follow the reaction paths either op-

timized for the ground electronic state S_0, or the first excited electronic state S_1, or the ground ionic state D_0.

Finally, CAS(12,12)/aug-cc-pVDZ calculations were performed for each stable geometry found at the MP2 level of theory. This was performed for both the 8Q/*cis*-8HQ/*trans*-8HQ and 6Q/*cis*-6HQ/*trans*-6HQ series of conformers, hence documenting their vertical excitation and ionization energies S_0-S_1, S_0-S_2, S_0-D_0 and S_0-D_1.

Note that only semiquantitative computational information is necessary for the interpretation of the present experimental data. This justifies the choice of using a limited active space in the CAS calculation. Of course if the present calculations were intended to be a step towards dynamical calculations, a much larger active space and inclusion of corrections for the dynamical electronic correlation would have been required as exemplified recently by Gonon and coworker for benzopyran, a molecule of similar size as 8HQ [32, 33]. Another issue could have been accurate comparisons with spectroscopic data as exemplified by Chen *et al.* also for molecules of similar size as those treated in the present work [34]. In that case extensive MRCI-F12/aug-cc-pVDZ would have been necessary. Again, such purposes were beyond the scope of the present calculations.

6 Acknowledgment

The authors are indebt to Olivier Poizat who pointed us towards dynamics studies of hydroxyquinoline molecules. The authors kindly thank Olivier Gobert, Michel Perdrix and Delphine Guillaumet for setting up and maintaining the SLIC/LUCA laser. They also thank Majdi Hochlaf for informative discussions on the present calculations. LP acknowledges ANR11-EQPX0005-ATTOLAB and ANR 09-JCJC-0090-01-CHROMADYNE for support.

7 Keywords

hydroxyquinoline, photoinduced proton transfer, real-time dynamics, femtosecond, time-resolved relaxation dynamics.

8 TOC

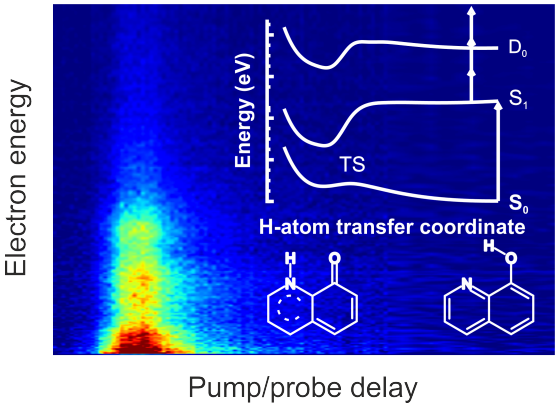

Figure 8: Graphical abstract showing essential features taken from Figs. 1, 2 and 7.

References

[1] M. Kasha. Proton-Transfer Spectroscopy. Perturbation of the Tautomerization Potential. *Journal of the Chemical Society, Faraday Transactions 2: Molecular and Chemical Physics*, 82:2379–2392, 1986.

[2] A. Müller. *Electron and Proton Transfer in Chemistry and Biology*. Elsevier, Amsterdam; New York, 1992.

[3] E. Bardez, A. Chatelain, B. Larrey, and B. Valeur. Photoinduced Coupled Proton and Electron Transfers. 1. 6-Hydroxyquinoline. *The Journal of Physical Chemistry*, 98:2357–2366, 1994.

[4] O. Poizat, E. Bardez, G. Buntinx, and V. Alain. Picosecond Dynamics of the Photoexcited 6-Methoxyquinoline and 6-Hydroxyquinoline Molecules in Solution. *J. Phys. Chem. A*, 108:1873–1880, 2004.

[5] H. N. Yu, O. H. Kwon, and D. J. Jang. Migration of Protons During the Excited-State Tautomerization of Aqueous 3-Hydroxyquinoline. *J. Phys. Chem. A*, 108:5932–5937, 2004.

[6] M. S. Mehata. Photoinduced Excited State Proton Rearrangement of 6-Hydroxyquinoline Along a Hydrogen-Bonded Acetic Acid Wire. *Chem. Phys. Lett.*, 436:357–361, 2007.

[7] M. S. Mehata. Proton Translocation and Electronic Relaxation Along a Hydrogen-Bonded Molecular Wire in a 6-Hydroxyquinoline/Acetic Acid Complex. *J. Phys. Chem. B*, 112:8383–8386, 2008.

[8] P. S. Sherin, N. P. Gritsan, and Y. P. Tsentalovich. Experimental and Quantum Chemical Study of Photochemical Properties of 4-Hydroxyquinoline. *Photochem. Photobiol. Sci.*, 8:1550–1557, 2009.

[9] I. Presiado, Y. Erez, R. Gepshtein, and D. Huppert. Excited-State Proton Transfer and Proton Reactions of 6-Hydroxyquinoline and 7-Hydroxyquinoline in Water and Ice. *J. Phys. Chem. C*, 113:20066–20075, 2009.

[10] N. Al-Lawatia, J. Husband, T. Steinbrecher, and O. K. Abou-Zied. Tautomerism in 7-Hydroxyquinoline: A Combined Experimental and Theoretical Study in Water. *J. Phys. Chem. A*, 115:4195–4201, 2011.

[11] M. S. Mehata, K. Awasthi, T. Iimori, and N. Ohta. Electric Field Effects on State Energy and Molecular Orientation of 2-Hydroxyquinoline in Solid Polymer Films. *Journal of Photochemistry and Photobiology a-Chemistry*, 204:39–45, 2009.

[12] H. J. Park, O. H. Kwon, C. S. Ah, and D. J. Jang. Excited-State Tautomerization Dynamics of 7-Hydroxyquinoline in Beta-Cyclodextrin. *J. Phys. Chem. B*, 109:3938–3943, 2005.

[13] O. H. Kwon, T. G. Kim, Y. S. Lee, and D. J. Jang. Biphasic Tautomerization Dynamics of Excited 7-Hydroxyquinoline in Reverse Micelles. *J. Phys. Chem. B*, 110:11997–12004, 2006.

[14] H. Mortada, V. Mazet, C. Soussen, C. Collet, and L. Poisson. Parameterized Source Separation for Delayed Spectroscopic Signals. *Signal Process.*, 158:48–60, 2019.

[15] C. Ruckebusch, M. Sliwa, P. Pernot, A. de Juan, and R. Tauler. Comprehensive Data Analysis of Femtosecond Transient Absorption Spectra: A Review. *Journal of Photochemistry and Photobiology C: Photochemistry Reviews*, 13:1–27, 2012.

[16] M. R. Panman, P. Bodis, D. J. Shaw, B. H. Bakker, A. C. Newton, E. R. Kay, D. A. Leigh, W. J. Buma, A. M. Brouwer, and S. Woutersen. Time-Resolved Vibrational Spectroscopy of a Molecular Shuttle. *Phys. Chem. Chem. Phys.*, 14:1865–1875, 2012.

[17] L. Poisson, D. Nandi, B. Soep, M. Hochlaf, M. Boggio-Pasqua, and J.-M. Mestdagh. A roaming wavepacket in the dynamics of electronically excited 2-hydroxypyridine. *Phys. Chem. Chem. Phys.*, 16:581, 2014.

[18] E. Bohl, B. Mignolet, J. O. Johansson, F. Remacle, and E. E. B. Campbell. Low-Lying, Rydberg States of Polycyclic Aromatic Hydrocarbons (Pahs) and Cyclic Alkanes. *Phys. Chem. Chem. Phys.*, 19:24090–24099, 2017.

[19] J. L. Gosselin and P. M. Weber. Rydberg fingerprint spectroscopy: A new spectroscopic tool with local and global structural sensitivity. *J. Phys. Chem. A*, 109:4899–4904, 2005.

[20] S. Awali, L. Poisson, B. Soep, M.-A. Gaveau, M. Briant, C. Pothier, J.-M. Mestdagh, M. Ben El Hadj Rhouma, M. Hochlaf, V. Mazet, and S. Faisan. Time resolved observation of the solvation dynamics of a rydberg excited molecule deposited on an argon cluster-i: Dabco(star) at short times. *Phys. Chem. Chem. Phys.*, 16:516–526, 2014.

[21] A. Lietard, G. Piani, L. Poisson, B. Soep, J.-M. Mestdagh, S. Aloise, A. Perrier, D. Jacquemin, and M. Takeshita. Competitive direct vs. indirect photochromism dynamics of constrained inverse dithienylethene molecules. *Phys. Chem. Chem. Phys.*, 16:22262–22272, 2014.

[22] A. Lietard, G. Piani, M. Briant, M.-A. Gaveau, S. Faisan, V. Mazet, B. Soep, J.-M. Mestdagh, and L. Poisson. Self-trapping relaxation decay investigated by time-resolved photoelectron spectroscopy. *Phys. Chem. Chem. Phys.*, 20:11206–11214, 2018.

[23] A. Eppink and D. H. Parker. Velocity map imaging of ions and electrons using electrostatic lenses: Application in photoelectron and photofragment ion imaging of molecular oxygen. *Rev. Sci. Instrum.*, 68:3477–3484, 1997.

[24] A. Stolow, A. E. Bragg, and D. M. Neumark. Femtosecond time-resolved photoelectron spectroscopy. *Chem. Rev.*, 104:1719–1757, 2004.

[25] G. A. Garcia, L. Nahon, and I. Powis. Two-dimensional charged particle image inversion using a polar basis function expansion. *Rev. Sci. Instrum.*, 75:4989–4996, 2004.

[26] A. V. Baklanov, L. M. C. Janssen, D. H. Parker, L. Poisson, B. Soep, J.-M. Mestdagh, and O. Gobert. Direct mapping of recoil in the ion-pair dissociation of molecular oxygen by a femtosecond depletion method. *J. Chem. Phys.*, 129, 2008.

[27] H. J. Werner, P. J. Knowles, G. Knizia, , F. R. Manby, M. Schütz, et al. Molpro, version 2010.1, a package of *ab-initio* programs - see http://www.molpro.net.

[28] R. D. Amos, J. S. Andrews, N. C. Handy, and P. J. Knowles. Open shell møller-plesset perturbation theory. *Chem. Phys. Lett.*, 185:256–264, 1991.

[29] T. H. Dunning. Gaussian basis sets for use in correlated molecular calculations. I. The atoms boron through neon and hydrogen. *J. Chem. Phys.*, 90:1007, 1989.

[30] P. J. Knowles and H. J. Werner. An efficient second order MCSCF method for long configuration expansions. *Chem. Phys. Lett.*, 115:259–267, 1985.

[31] H. J. Werner and P. J. Knowles. A second order MCSCF method with optimum convergence. *J. Chem. Phys.*, 82:5053, 1985.

[32] Benjamin Gonon. *Simulations quantiques non-adiabatiques d'un photo-interrupteur moléculaire vers un dialogue expérience-théorie.* PhD thesis, Université de Montpellier, 2017.

[33] B. Gonon, B. Lasorne, G. Karras, L. Joubert-Doriol, D. Lauvergnat, F. Billard, B. Lavorel, O. Faucher, S. Guérin, E. Hertz, and F. Gatti. A generalized vibronic-coupling hamiltonian for molecules without symmetry: Application to the photoisomerization of benzopyran. *J. Chem. Phys.*, 150:124109, 2019.

[34] Z. Chen, K.-C. Lau, G. A. Garcia, L. Nahon, D. K. Božanic, L. Poisson, M. M. Al-Mogren, M. Schwell, J. S. Francisco, A. Bellili, and M. Hochlaf. Identifying cytosine-specific isomers via high-accuracy single photon ionization. *J. Am. Chem. Soc.*, 138:16596–16599, 2016.